Available online at www.sciencedirect.com
ScienceDirect
Applied Catalysis B: Environmental 81 (2008) 115–121
APPLIED CATALYSIS B: ENVIRONMENTAL
www.elsevier.com/locate/apcatb

Pt/MnO_x–CeO_2 catalysts for the complete oxidation of formaldehyde at ambient temperature

Xingfu Tang [1], Junli Chen, Xiumin Huang, Yide Xu, Wenjie Shen *

State Key Laboratory of Catalysis, Dalian Institute of Chemical Physics, Chinese Academy of Sciences, 457 Zhangshan Road, Dalian 116023, China

Received 26 August 2006; received in revised form 12 December 2007; accepted 12 December 2007
Available online 23 December 2007

Abstract

MnO_x–CeO_2 mixed oxides with a Mn/(Mn + Ce) molar ratios of 0–1 were prepared by a modified coprecipitation method and investigated for the complete oxidation of formaldehyde. The MnO_x–CeO_2 with Mn/(Mn + Ce) molar ratio of 0.5 exhibited the highest catalytic activity among the MnO_x–CeO_2 mixed oxides. Structure analysis by X-ray powder diffraction and temperature-programmed reduction of hydrogen revealed that the formation of MnO_x–CeO_2 solid solution greatly improved the low-temperature reducibility, resulting in a higher catalytic activity for the oxidation of formaldehyde. Promoting effect of Pt on the MnO_x–CeO_2 mixed oxide indicated that both the Pt precursors and the reduction temperature greatly affected the catalytic performance. Pt/MnO_x–CeO_2 catalyst prepared from chlorine-free precursor showed extremely high activity and stability after pretreatment with hydrogen at 473 K. 100% conversion of formaldehyde was achieved at ambient temperature and no deactivation was observed for 120 h time-on-stream. The promoting effect of Pt was ascribed to enhance the effective activation of oxygen molecule on the MnO_x–CeO_2 support.

Keywords: MnO_x–CeO_2 mixed oxides; Pt/MnO_x–CeO_2 catalyst; Complete oxidation; Formaldehyde; Platinum precursor

1. Introduction

Formaldehyde emitted from the widely used construction and decoration materials is becoming one of the major indoor pollutants in airtight buildings. Long-term exposure to the air even containing a few ppm of HCHO could cause adverse effects on the eyes and respiratory system [1]. Thus, great efforts have been made to reduce the indoor emission of HCHO for satisfying the stringent environmental regulations. Conventional physical absorption and/or chemical reactions with impregnated potassium permanganate and organic amines were proved to be efficient for HCHO elimination at field experiments, but these adsorbents were effective for only a short period due to their limited removal capacities [2,3].

Heterogeneous catalytic oxidation of HCHO is regarded as one of the most promising technologies for indoor air purification. However, the development of effective catalysts possessing high activity for the complete oxidation of HCHO with very low concentrations into harmless CO_2 and water at ambient temperature is still the main challenge. Supported noble metals were demonstrated to be promising for the complete oxidation of HCHO at low temperatures and even at ambient temperature. For example, complete oxidation of HCHO was obtained over a Ru/CeO_2 catalyst at 473 K [4]. Pd–Mn/Al_2O_3 catalysts were recently reported to possess high activity for the complete oxidation of HCHO at about 363 K in air stream [5]. Pt supported on ceramics also gave 100% conversion of HCHO at about 423 K [6]. Recent studies on the adsorption and oxidation of HCHO over supported noble metal (Pt, Rh, Pd or Au) catalysts made significant progress on lowering the reaction temperature [7–10], and particularly the Pt/TiO_2 catalyst was found to be active enough to oxidize HCHO into CO_2 and H_2O even at ambient temperature [9,10].

It was also demonstrated that transition metal oxides, like MnO_x and CeO_2, could show catalytic activities as high as or slightly higher than those of the supported noble metals for

* Corresponding author. Tel.: +86 411 84379085; fax: +86 411 84694447.
E-mail address: shen98@dicp.ac.cn (W. Shen).
[1] Present address: Department of Environmental Science and Engineering, Tsinghua University, Beijing 100084, China.

0926-3373/$ – see front matter © 2007 Elsevier B.V. All rights reserved.
doi:10.1016/j.apcatb.2007.12.007

oxidation of formaldehyde [11]. MnO_x–CeO_2 mixed oxides, as environmental-friendly catalysts, have been extensively studied for the wet oxidation of ammonia [12], phenol [13] and acrylic acid [14]. It was revealed that the chemical composition of the MnO_x–CeO_2 mixed oxides greatly influenced the catalyst activity, and the optimum composition often depended on the nature of the reactants. MnO_x–CeO_2 with a Mn/(Mn + Ce) molar ratio of 0.5 was found to be more active for the oxidation reactions of phenol [13] and polyethylene glycol [15], due to the synergetic effect through the interaction between the mixed oxides. Promoting effect of noble metals on the MnO_x–CeO_2 mixed oxides also has been investigated to enhance the catalytic performance. Imamura et al. [16] reported that the addition of Ru to MnO_x–CeO_2 resulted in a significant increase in the catalytic activity for the wet-oxidation of a model domestic wastewater. Pt promotion of MnO_x–CeO_2 enhanced the CO_2 selectivity and reduced the amount of carbon deposits in the deep oxidation of phenol, which were ascribed to great improvement in the redox properties of MnO_x–CeO_2 by Pt [17,18].

We recently reported that MnO_x–CeO_2 mixed oxides could exhibit high catalytic activity for the complete oxidation of HCHO at 373 K [19]. In this work, we extended to study the effects of the chemical composition of the MnO_x–CeO_2 mixed oxides and the promoting effect of Pt on the catalytic activity for HCHO oxidation. Structure analysis of the catalysts were performed with N_2 adsorption, X-ray powder diffraction (XRD) and H_2 temperature-programmed reduction (H_2-TPR), and subsequently correlated with their catalytic performances.

2. Experimental

2.1. Catalyst preparation

MnO_x–CeO_2 mixed oxides with Mn/(Mn + Ce) molar ratios of 0 to 1 were prepared by a modified coprecipitation method, as described elsewhere [19]. Briefly, 2 M KOH aqueous solution was slowly added to an aqueous solution containing $Mn(NO_3)_2{\cdot}6H_2O$, $KMnO_4$ and $(NH_4)_2Ce(NO_3)_6$ at 323 K until the pH value of the mixture reached 10.5 under vigorous stirring. The molar ratio of $Mn(NO_3)_2{\cdot}6H_2O$ to $KMnO_4$ was kept at 3:2. The precipitate was further aged at 323 K for 2 h in the mother liquid. After filtrating and washing with distilled water, the obtained solid was dried at 383 K for 12 h and calcined at 773 K for 6 h in air.

Two Pt/MnO_x–CeO_2 catalysts were then prepared by the conventional impregnation process. The MnO_x–CeO_2 powder with a Mn/(Mn + Ce) molar ratio of 0.5 was added to an aqueous solution of H_2PtCl_6 or $Pt(NH_3)_2(NO_2)_2$ containing 3 wt.% of platinum with respect to the MnO_x–CeO_2. The mixture was evaporated with a rotary evaporator at 323 K to remove water, and the obtained solid was then dried at 383 K for 12 h and finally calcined at 673 K for 4 h in air. These Pt/MnO_x–CeO_2 catalysts were designated as Pt–Cl (prepared from H_2PtCl_6) and Pd–N (prepared from $Pt(NH_3)_2(NO_2)_2$), respectively.

2.2. Catalyst characterization

BET surface areas of the samples were measured by N_2 adsorption–desorption isotherms at 77 K using a Micromeritics ASAP 2000 instrument. Prior to the measurement, the samples were degassed at 573 K for 2 h.

Elemental analysis was performed by inductively coupled plasma atomic emission spectroscopy (ICP-AES) on a Plasam-Spec-I spectrometer.

X-ray powder diffraction patterns were recorded with a D/Max-2500/PC diffractometer (Rigaku, Japan) operated at 40 kV and 250 mA, using nickel-filtered Cu Kα (λ = 0.15418 nm) radiation. The lattice parameters were calculated according to the Cohen procedure [20].

Hydrogen temperature-programmed reduction (H_2-TPR) measurements were carried out on a CHEMBET 3000 adsorption instrument (Quantachrome, USA) equipped with a TCD detector. 30–50 mg samples were loaded and pretreated with He at 573 K for 1 h to remove the adsorbed carbonates and hydrates. After cooling to room temperature and introducing the reduction agent of a 5% H_2/Ar mixture with a flow rate of 50 mL/min, the temperature was then programmed to rise at a ramp of 10 K/min. A calibration curve of the TCD response signal expressed by the integral area of the peak as a function of the amount of the hydrogen consumption was established by reducing known amounts of pure CuO to Cu. For the determination of the oxidation state of manganese in the samples, MnO was assumed to be the final state after the reduction at temperatures below 1173 K [21].

2.3. Activity measurement

The oxidation of HCHO was performed in a continuous flow fixed-bed reactor under atmospheric pressure. 200 mg catalyst (40–60 mesh) was sandwiched by quartz wool layers in a quartz tube reactor. Typically, the MnO_x–CeO_2 mixed oxides were used as-prepared, and the Pt/MnO_x–CeO_2 catalysts were pretreated with hydrogen at 473 K for 1 h. Gaseous HCHO was generated by flowing He coming from a mass-flow controller through paraformaldehyde (96%, ACROS ORGANICS) in an incubator. The temperature of the incubator and/or the flow rate of He gas were adjusted to obtain desired concentration of HCHO (30–580 ppm). The HCHO-containing stream was then mixed with the main gas stream of 20 vol.% O_2/He, which was introduced through another mass-flow controller. The gas hourly space velocity (GHSV) was 30,000 mL/g_{cat} h. Effluents from the reactor were analyzed by on-line HP 6890 gas chromatograph equipped with TCD and FID. To determine the exact concentration of produced carbon dioxide, a nickel catalyst converter was placed before the FID and used for converting CO_2 quantitatively into methane in the presence of hydrogen. In typical runs, the reaction data were obtained after HCHO oxidation was performed for 3 h in order to achieve the steady state. No other carbon-containing compounds except CO_2 in the products were detected for all the tested catalysts.

3. Results and discussion

3.1. MnO_x–CeO_2 mixed oxides

Fig. 1 shows the HCHO conversions over the MnO_x–CeO_2 mixed oxides as a function of Mn/(Mn + Ce) molar ratio at 363 K. Obviously, the chemical composition of the MnO_x–CeO_2 mixed oxides significantly affected the catalytic activities for the oxidation of HCHO. Pure CeO_2 gave formaldehyde conversion less than 10%, and slightly increased HCHO conversion (12%) was observed when the Mn/(Mn + Ce) molar ratio increased to 0.1. Rapid increase in HCHO conversion was obtained as the Mn/(Mn + Ce) molar ratio further increased, and the maximum value of 90% was achieved with the Mn/(Mn + Ce) molar ratio of 0.5, followed by gradually decreased HCHO conversion with the Mn/(Mn + Ce) molar ratio. Consequently, the MnO_x–CeO_2 with Mn/(Mn + Ce) molar ratio of 0.5 showed the highest catalytic activity, over which more than 90% of HCHO conversion were achieved.

Fig. 2 compares the surface areas of the MnO_x–CeO_2 mixed oxides with the specific reaction rates of HCHO. Clearly, the specific reaction rate of HCHO based on per unit surface area increased monotonically with increasing the molar ratio of Mn/(Mn + Ce). This suggested that MnO_x was the active species, and CeO_2 acted as a support or a promoting component in the MnO_x–CeO_2 mixed oxides.

Fig. 3 shows the XRD patterns of the MnO_x–CeO_2 mixed oxides. For the samples with the molar ratio of Mn/(Mn + Ce) $\leq$ 0.5, the XRD patterns did not show any diffraction of manganese oxides, and only broad peaks due to CeO_2 of a cubic fluorite structure were observed. This is in good consistent with the recent reports concerning the structure features of MnO_x–CeO_2 mixed oxides, which found that the phase composition of manganese and cerium mixed oxides strongly depended on the molar ratios of manganese and cerium oxides [22]. The diffraction patterns of MnO_x–CeO_2 mixed oxides at Mn/(Mn + Ce) $\geq$ 0.75 showed crystallization of MnO_x, whereas those at Mn/(Mn + Ce) $\leq$ 0.5 consisted of only broad peaks attributed to CeO_2 due to the formation of solid solution between MnO_x and CeO_2. For the MnO_x–CeO_2 mixed oxides with Mn/(Mn + Ce) > 0.5, the intensive and sharp diffractions representing MnO_2 appeared in addition to the increasing broad diffraction peaks of ceria, indicating that the presence of separated MnO_2. Meanwhile, the intensity of the diffraction peaks of MnO_2 also increased with increasing Mn content. Table 1 summarizes the lattice parameters of the cubic fluorite-type structure for the MnO_x–CeO_2 mixed oxides. Apparently, the calculated lattice parameters of the MnO_x–CeO_2 mixed oxides gradually decreased from 0.5416 nm (for pure CeO_2) to 0.5376 nm when the Mn/(Mn + Ce) molar ratio increased from 0 to 0.5. This suggested that manganese ions were probably incorporated into the ceria lattice and led to the formation of solid solution between manganese and cerium oxides by considering the fact that the ionic radius of Mn^{4+} (0.053 nm) is smaller than that of Ce^{4+} (0.094 nm) [22].

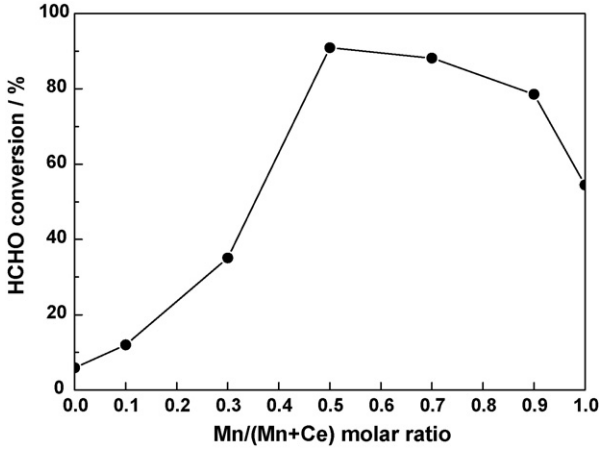

Fig. 1. Dependence of HCHO conversion on Mn/(Mn + Ce) molar ratio in the MnO_x–CeO_2 mixed oxides. Reaction temperature = 363 K, HCHO = 580 ppm, O_2 = 20.0 vol.%, He balance, GHSV = 30,000 mL/g_{cat} h.

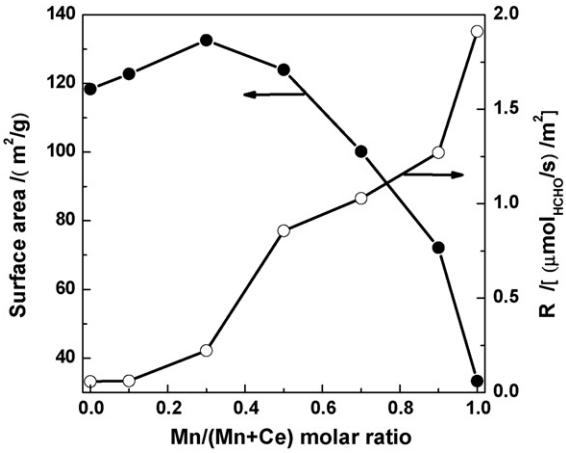

Fig. 2. Surface areas of the MnO_x–CeO_2 mixed oxides and the specific reaction rates of HCHO oxidation. Reaction temperature = 363 K, HCHO = 580 ppm, O_2 = 20.0 vol.%, He balance, GHSV = 30,000 mL/g_{cat} h.

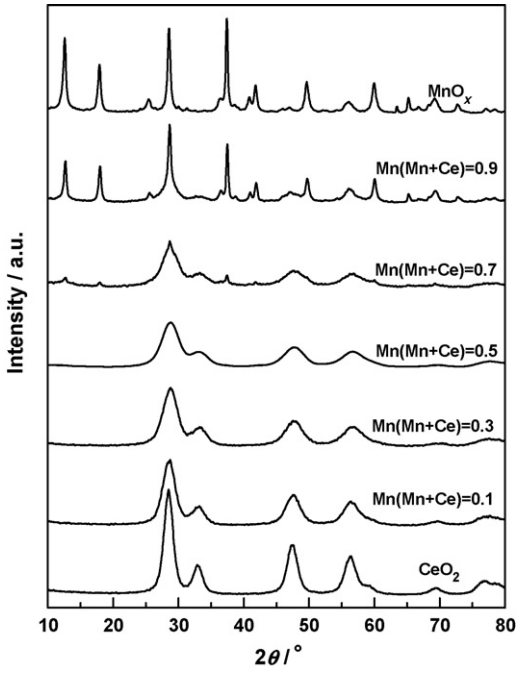

Fig. 3. XRD patterns of the MnO_x–CeO_2 mixed oxides.

Table 1
Lattice parameters and H_2-TPR results of the MnO_x–CeO_2 mixed oxides

Mn/(Mn + Ce) ratio	Lattice parameter (nm)[a]	Consumed hydrogen (μmol/g)[b]
0	0.5416	726
0.1	0.5410	1,273
0.3	0.5385	2,547
0.5	0.5376	4,191
0.7	–	6,288
0.9	–	9,156
1.0	–	10,795

[a] Calculated from XRD patterns (Fig. 3).
[b] Calculated from H_2-TPR profiles (Fig. 4).

Fig. 4 shows the H_2-TPR profiles of the MnO_x–CeO_2 mixed oxides. Pure CeO_2 exhibited a weak and broad reduction peak at about 850 K, corresponding the removal of surface oxygen of ceria [19,23]. The H_2-TPR profile of MnO_2 showed two overlapped reduction peaks at 623–843 K with a slight shoulder at about 590 K. As we previously reported [19], the shoulder reduction peak was related to the readily reducible small clusters of surface manganese oxides, and the two intensive and broad peaks represented the consequential reductions of MnO_2 to Mn_3O_4 and Mn_3O_4 to MnO, respectively. Two reduction peaks of the MnO_x–CeO_2 mixed oxides were clearly observed. The low-temperature reduction peak corresponded to the reduction of MnO_2 to Mn_3O_4, and the high-temperature reduction peak represented the combined reduction of Mn_3O_4 to MnO and surface Ce^{4+} to Ce^{3+} species [19]. Noticeably, the low-temperature reduction peak of the MnO_x–CeO_2 mixed oxides systematically shifted to lower temperatures with increasing Ce content, whereas no remarkable shift of the high-temperature reduction peak could be evidenced. This result indicates that the addition of ceria to manganese oxide accelerated the mobility of surface oxygen species and facilitated the reduction of manganese oxide from MnO_2 to Mn_3O_4. Table 1 also summarizes the amounts of hydrogen consumed during the TPR measurements. The total hydrogen consumption amount of CeO_2 was 726 μmol/g, corresponding to a stoichiometric change in the composition of CeO_2 to $CeO_{1.88}$. The total amount of consumed hydrogen for MnO_2 was 10,795 μmol/g, from which the predominant manganese species was estimated to be Mn^{4+} by assuming that MnO was the final reduction state [21]. For the MnO_x–CeO_2 mixed oxides, the total amount of consumed hydrogen increased with increasing Mn content, and the oxidation state of manganese was calculated to be about 4.0 for all the samples. This may suggest that the manganese species is mainly Mn^{4+} in the MnO_x–CeO_2 mixed oxides, irrespective of their chemical compositions.

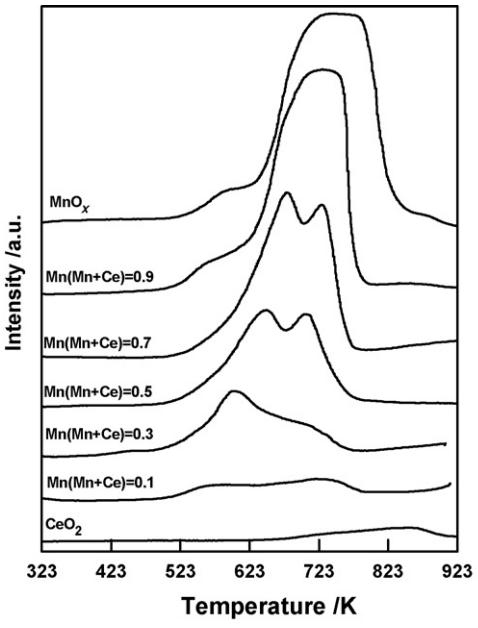

Fig. 4. H_2-TPR profiles of the MnO_x–CeO_2 mixed oxides.

As a matter of fact, the interaction between MnO_x and CeO_2 in the MnO_x–CeO_2 mixed oxides plays a crucial role in the oxidation reaction. Imamura et al. [24] evidenced the existence of a synergistic mechanism between the manganese and cerium oxides in the MnO_x–CeO_2 composite by comparing the catalytic activity with that of a physical mixture of MnO_x and CeO_2 for wet air oxidation of ammonia. Ding et al. [12] further developed a chain of reactions to explain this synergistic mechanism, which was also verified for the selective reduction of NO by NH_3 by Yang et al. [25]. This synergistic mechanism can be essentially regarded as a process of oxygen activation, and the oxygen transfer through the redox recycles of Mn^{4+}/Mn^{3+} and Ce^{4+}/Ce^{3+} was proposed as follows.

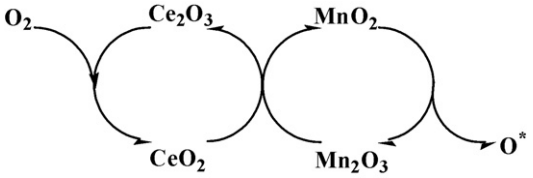

Thus, the oxygen transfer from molecular oxygen to active sites of MnO_2 through oxygen reservoir CeO_2 achieved the effective activation of molecular oxygen in the feed stream. Meanwhile, the higher density of manganese species as active sites and the higher manganese oxidation state were equally important for the oxidation reaction, as we previously stated [19]. It is reasonable to say that the presence of separated MnO_2 in the MnO_x–CeO_2 mixed oxides with Mn/(Mn + Ce) > 0.5 and the relative lower concentration of manganese species for in the MnO_x–CeO_2 mixed oxides with Mn/(Mn + Ce) < 0.5 were the major reasons causing the decrease of activity for HCHO oxidation. The MnO_x–CeO_2 with a Mn/(Mn + Ce) molar ratio of 0.5, favoring the formation of a solid solution, provided strong interaction between MnO_x and CeO_2 and relatively high density of manganese species, which accounted for the highest activity among the MnO_x–CeO_2 mixed oxides.

3.2. *Pt/MnO_x–CeO_2 catalysts*

Pt loading on the MnO_x–CeO_2 with a Mn/(Mn + Ce) ratio of 0.5 only slightly decreased the BET surface area of the support (124 m^2/g) and the specific surface areas of the Pt/MnO_x–CeO_2

catalysts were nearly identical (around 105 m^2/g). When the reaction was performed at ambient temperature with the feed gas composition of 30 ppm HCHO and 20 vol.% O_2 balanced by He, the bare support only gave HCHO conversion of 26%. The Pt/MnO_x–CeO_2 catalysts greatly improved the catalytic performance, and the HCHO conversion strongly depended on the nature of Pt precursors. The Pt–N catalyst prepared from $Pt(NH_3)_2(NO_2)_2$ showed extremely high activity, over which HCHO was completely oxidized into CO_2 and H_2O. But the Pt–Cl catalyst prepared from H_2PtCl_6 only gave 28% of HCHO conversion under the same reaction conditions. This lower HCHO conversion should be associated to the inhibiting effect of chlorine anions remaining on the surface of the catalyst after pretreatment. Similar phenomenon has been reported for the complete oxidation reactions of hydrocarbons and CO [26–28]. Gracia et al. [28] investigated the poisoning effect of chlorine on the activity of supported Pt catalysts for the oxidations of CO, methane and ethane and found that the residual chlorine was mobile under the reaction conditions and led to deactivation by blocking the active sites on the Pt surface.

Fig. 5 shows the XRD patterns of the Pt/MnO_x–CeO_2 catalysts reduced with hydrogen at 473 K. The characteristic diffractions of the Pt/MnO_x–CeO_2 catalysts were similar to the MnO_x–CeO_2 (shown in Fig. 3), and no diffraction peaks due to the platinum species could be observed, indicating that the platinum species were highly dispersed on the surface of MnO_x–CeO_2.

Fig. 6 displays the H_2-TPR profiles of the Pt/MnO_x–CeO_2 catalysts. Compared with the TPR behavior of the MnO_x–CeO_2 (shown in Fig. 4), the addition of platinum dramatically modified the reduction features of the MnO_x–CeO_2 mixed oxide, depending on the nature of the Pt precursor. The Pt–Cl catalyst showed one broad and intensive reduction peak at 560–643 K, while the Pt–N catalyst only exhibited one intensive reduction peak at about 532 K. Obviously, the reduction temperatures symmetrically shifted to lower regions, and this phenomenon is often interpreted in terms of the activation and spillover of hydrogen from the initially reduced Pt to MnO_x–CeO_2, and facilitated the reduction of the oxides [18,23]. Similar reduction character was also observed over Pd/MnO_x–

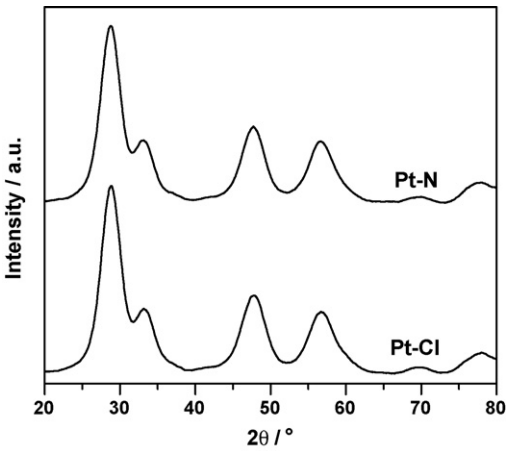

Fig. 5. XRD patterns of the Pt/Mn_x–CeO_2 catalysts.

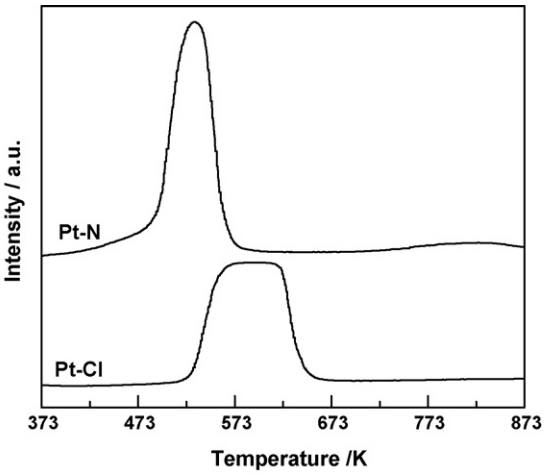

Fig. 6. H_2-TPR profiles of the Pt/MnO_x–CeO_2 catalysts.

CeO_2 catalysts [17]. The amounts of hydrogen consumed by the Pt–N and Pt–Cl catalysts during the H_2-TPR processes were 4168 and 4156 μmol/g, respectively. It could be seen that the total amount of consumed hydrogen over the Pt/MnO_x–CeO_2 catalysts only marginally decreased when compared with the MnO_x–CeO_2 support (4191 μmol/g), indicating that the oxidation state of manganese and cerium remained unchanged after Pt loading.

The nature of Pt precursor was also previously found to influence the reducibility of Pt-containing catalysts. Lieske et al. [29] have identified the formation of oxychloroplatinum species, PtO_xCl_y, on the Pt catalysts prepared from chlorinated salts, which was further confirmed by Marceau et al. [30]. It has been reported that the reduction of the PtO_xCl_y species occurred at higher temperatures than PtO_x species [31]. Gracia et al. [28] further verified the transport and mobility of residual chlorine anions between Pt and the supports by EXAFS and IR measurements. Moreover, the presence of residual Cl^- species may also lead to the formation CeOCl species, which would greatly decrease the redox ability of the MnO_x–CeO_2 support. Kepinski and Oka [32] studied the influence of chlorine in a Pd(Cl)/CeO_2 catalyst during reduction with hydrogen and found that CeOCl crystallites formed on the surface faces of CeO_2 crystals even at 573 K through the incorporation of Cl^- into the oxygen vacancies at the CeO_2 surface. Although the presence of noble metal is not necessary for CeOCl formation, it facilitated the surface reduction of CeO_2 at low temperatures by hydrogen spillover and thus lowers the temperature of CeOCl formation.

Thus, it seems true that the presence of residual chlorine in the Pt–Cl catalyst not only retarded the reduction of Pt species, but also migrated to the MnO_x–CeO_2 support and replaced the oxygen vacancy of ceria through the formation of CeOCl phase. This caused the reduction of the Pt–Cl catalyst occur at higher temperatures, and consequently the oxidation of HCHO on the Pt–Cl catalyst was more difficult than that on the Pt–N catalyst at ambient temperature.

Fig. 7 shows the effect of reduction temperature on the catalytic activity of the Pt–N catalyst for HCHO oxidation at ambient temperature. The as-prepared Pt–N catalyst only gave 14% HCHO conversion, even lower than that (26%) of the

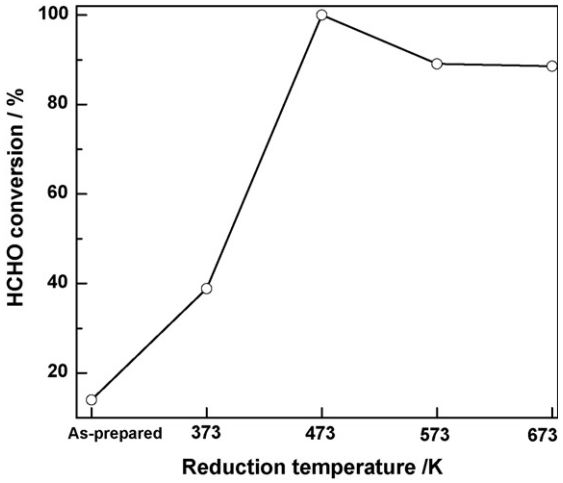

Fig. 7. Effect of the reduction temperature on the catalytic activity of the Pt–N catalyst. Reaction temperature = 298 K, HCHO = 30 ppm, O_2 = 20.0 vol.%, He balance, GHSV = 30,000 mL/g_{cat} h.

MnO_x–CeO_2 support. HCHO conversion substantially increased to approximately 40% after the pretreatment with hydrogen at 373K. When the reduction temperature was increased to 473 K, HCHO conversion rapidly increased up to 100%, followed by slightly decreasing as the reduction temperature increased to 573 K. Further increase of the reduction temperature to 673 K appeared no additional effect on the catalytic activity.

Depending on the nature of the reactants to be treated, the different active states of the Pt-containing catalysts showed very different catalytic activity. It was generally accepted that the reduced state of Pt was more active than the oxidized state [28,33]. Gracia et al. [28] found that the catalytic activity could be closely correlated with the amount of exposed metallic Pt in a Pt/Al_2O_3 catalyst, and the highest activity for CO oxidation was obtained on the reduced catalyst, while the calcined catalyst showed very poor activity. Here, we propose that the metallic Pt should be the most active phase for HCHO oxidation in the Pt–N catalyst. When the reduction temperature gradually increased to 473 K, the enhancement of catalytic activity probably resulted from the increase of the amount of metallic Pt, because of the complete reduction of PtO_x at about 473 K [18]. Meanwhile, the oxygen transfer in MnO_x–CeO_2 was also crucial for HCHO oxidation. When the reduction was performed at 573 K, the slight decrease of the catalytic activity appeared to be due to the reduction of MnO_x–CeO_2 (Fig. 6), which suppressed the effective activation of oxygen molecules in the feed stream. However, the catalytic activity did not further decrease when the Pt–N catalyst was reduced at 673 K. This can be understood by considering the fact that the reducibility of the MnO_x–CeO_2 support did not change with increasing the reduction temperature from 573 to 673 K, as confirmed by the H_2-TPR profile of the Pt–N catalyst in Fig. 6. Therefore, reduction of the Pt–N catalyst with hydrogen at 473 K resulted in the formation of metallic Pt, but it did not induce the reduction of the MnO_x–CeO_2 support. This optimal metal–support interface will favor the preferential adsorption of formaldehyde on Pt and the effective activation of oxygen molecule on MnO_x–CeO_2, over which HCHO was completely oxidized into CO_2 and H_2O at ambient temperature.

Pt/TiO_2 was recently found to be the most active system among TiO_2 supported noble metals (Pt, Rh, Pd and Au) for HCHO oxidation, over which 100% conversion of formaldehyde was achieved at room temperature [9,10]. FTIR studies on the adsorption and reaction of formaldehyde over TiO_2 supported Pt and Rh catalysts have revealed that formate species can be easily formed upon formaldehyde adsorption, and the sequent conversion of surface formate to CO seemed to be the rate-determining step for the catalytic oxidation of HCHO, which was significantly promoted by the presence of precious metals [10,34,35]. Accordingly, it can be assumed that the oxidation of formaldehyde on the Pt/MnO_x–CeO_2 catalyst follows a similar reaction pathway. The optimal interface between Pt and MnO_x–CeO_2 formed by proper pretreatment would play an essential role in this mechanism, where the effective activation of oxygen molecule on MnO_x–CeO_2 favored the initial oxidation of formaldehyde to formate species [36] and the Pt nearby facilitated the decomposition of the formate to CO and subsequently the oxidation of CO into CO_2 even at ambient temperature.

The effect of HCHO concentration was further investigated over the Pt–N catalyst which was pre-reduced with hydrogen at 473 K. Fig. 8 shows the HCHO conversions over the Pt–N catalyst with different HCHO concentrations in the feed gas at ambient temperature. 100% conversion of HCHO was achieved when HCHO concentration was below 100 ppm, which slightly decreased as HCHO concentration increased, but more than 50% HCHO conversion could still be obtained with further increase of HCHO concentration to 580 ppm.

Fig. 9 illustrates the HCHO conversion with time-on-stream at ambient temperature over the Pt–N catalyst pre-reduced with hydrogen at 473 K. Clearly, complete conversion of HCHO into CO_2 and water remained unchanged and no deactivation could be observed even after 120 h time-on-stream. This result indicated the Pt–N catalyst is quite stable under the HCHO oxidation atmosphere at ambient temperature.

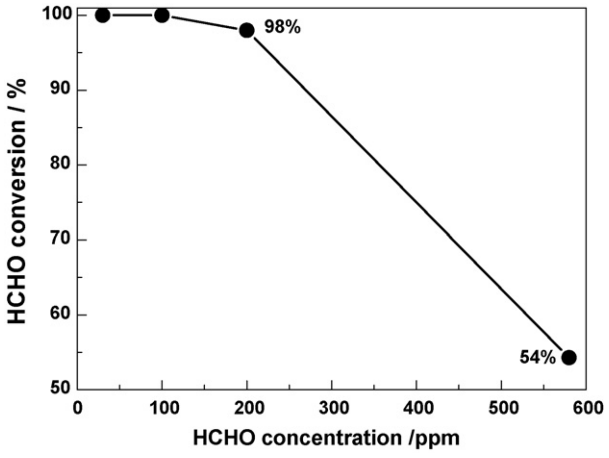

Fig. 8. Effect of HCHO concentration on the catalytic activity of the Pt–N catalyst. Reaction temperature = 298 K, O_2 = 20.0 vol.%, He balance, GHSV = 30,000 mL/g_{cat} h.

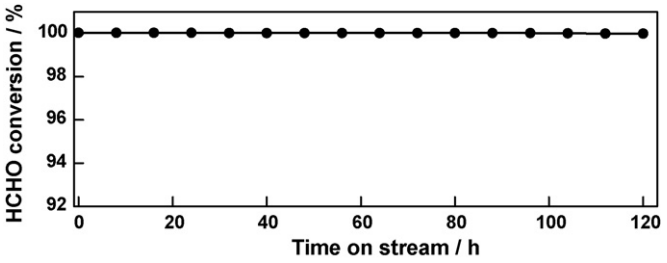

Fig. 9. HCHO conversion with time on stream over the Pt–N catalyst. Reaction temperature = 298 K, HCHO = 30 ppm, O_2 = 20.0 vol.%, He balance, GHSV = 30,000 mL/g_{cat} h.

4. Conclusions

Investigation on the chemical composition of the MnO_x–CeO_2 mixed oxides revealed that the MnO_x–CeO_2 mixed oxide with a Mn/(Mn + Ce) molar ratio of 0.5 exhibited the most promising catalytic activity for formaldehyde oxidation due to the strong interaction between MnO_2 and CeO_2 and the relative high density of manganese species. Promoting effect of Pt on the MnO_x–CeO_2 mixed oxide indicated that both the Pt precursors and the reduction temperature significantly affected the catalytic performance of the Pt/MnO_x–CeO_2 catalysts. The catalyst prepared from chlorine-free precursor and reduced at 473 K with hydrogen showed extremely high catalytic activity and could completely oxidize formaldehyde into CO_2 and H_2O at ambient temperature, and no deactivation was observed even for 120 h time-on-stream operation. The Pt promoting effect was interpreted by the presence of the active Pt for HCHO adsorption and the effective activation of oxygen molecule on MnO_x–CeO_2 by proper pretreatment.

References

[1] Y. Sekine, Atmos. Environ. 36 (2002) 5543–5547.
[2] R.J. Shaughnessy, E. Levetin, J. Blocker, K.L. Sublette, Indoor Air 4 (1994) 179–188.
[3] H. Nakayama, A. Hayashi, T. Eguchi, N. Nakamura, M. Tsuhako, Solid State Sci. 4 (2002) 1067–1070.
[4] S. Imamura, Y. Uematsu, K. Utani, T. Ito, Ind. Eng. Chem. Res. 30 (1991) 18–21.
[5] M.C. Álvarez-Galván, B. Pawelec, V.A. de la Peña O'Shea, J.L.G. Fierro, P.L. Arias, Appl. Catal. B 51 (2004) 83–91.
[6] K. Chuang, B. Zhou, S. Tong, Ind. Eng. Chem. Res. 33 (1994) 1680–1686.
[7] T. Kecskés, J. Raskó, J. Kiss, Appl. Catal. A 273 (2004) 55–62.
[8] C. Zhang, H. He, K. Tanaka, Catal. Commun. 6 (2005) 211–214.
[9] C. Zhang, H. He, K. Tanaka, Appl. Catal. B 65 (2006) 37–43.
[10] C. Zhang, H. He, Catal. Today 126 (2007) 345–350.
[11] Y. Sekine, A. Nishimura, Atmos. Environ. 35 (2001) 2001–2007.
[12] Z. Ding, L. Wade, E. Gloyna, Ind. Eng. Chem. Res. 37 (1998) 1707–1716.
[13] H. Chen, A. Sayari, A. Adnot, F. Larachi, Appl. Catal. B 32 (2001) 195–204.
[14] A.M.T. Silva, R.R.N. Marques, R.M. Quinta-Ferreira, Appl. Catal. B 47 (2004) 269–279.
[15] S. Imamura, Ind. Eng. Chem. Res. 38 (1999) 1743–1753.
[16] S. Imamura, Y. Okumura, T. Nishio, K. Utani, Y. Matsumura, Ind. Eng. Chem. Res. 37 (1998) 1136–1139.
[17] S. Hamoudi, F. Larachi, G. Cerrella, M. Cassanello, Ind. Eng. Chem. Res. 37 (1998) 3561–3566.
[18] S. Hamoudi, A. Sayari, K. Belkacemi, L. Bonneviot, F. Larachi, Catal. Today 62 (2000) 379–388.
[19] X. Tang, Y. Li, X. Huang, Y. Xu, H. Zhu, J. Wang, W. Shen, Appl. Catal. B 62 (2006) 265–273.
[20] H.P. Klug, L.E. Alexander, X-ray Diffraction Procedures, John Wiley, New York, 1954.
[21] F. Kapteijn, L. Singoredjo, A. Andreini, Appl. Catal. B 3 (1994) 173–189.
[22] M. Machida, M. Uto, D. Kurogi, T. Kijima, Chem. Mater. 12 (2000) 3158–3164.
[23] A. Trovarelli, Catal. Rev. Sci. Eng. 38 (1996) 439–520.
[24] S. Imamura, A. Dol, S. Ishido, Ind. Eng. Chem. Prod. Res. Dev. 24 (1985) 75–80.
[25] G. Qi, R. Yang, R. Chang, Appl. Catal. B 51 (2004) 93–106.
[26] M. Paulis, H. Peyrard, M. Montes, J. Catal. 199 (2001) 30–40.
[27] H. Karhu, A. Kalantar, I.J. Väyrynen, T. Salmi, D.Y. Murzin, Appl. Catal. A 247 (2003) 283–294.
[28] F.J. Gracia, J.T. Miller, A.J. Kropf, E.E. Wolf, J. Catal. 209 (2002) 341–354.
[29] H. Lieske, G. Lietz, H. Spindler, J. Volter, J. Catal. 81 (1983) 8–16.
[30] E. Marceau, M. Che, J. Saint-Just, J.M. Tatibouët, Catal. Today 29 (1996) 415–419.
[31] C. Contescu, D. Macovei, C. Craiu, C. Teodorescu, J.A. Schwarz, Langmuir 11 (1995) 2031–2040.
[32] L. Kepinski, J. Okal, J. Catal. 192 (2000) 48–53.
[33] S. Yang, A. Maroto-Valiente, M. Benito-Gonzalez, I. Rodriguez-Ramos, A. Guerrero-Ruiz, Appl. Catal. B 28 (2000) 223–233.
[34] J. Raskó, T. Kecskés, J. Kiss, J. Catal. 226 (2004) 183–191.
[35] J. Raskó, T. Kecskés, J. Kiss, J. Catal. 224 (2004) 261–268.
[36] C. Li, K. Domen, K. Maruya, T. Onishi, J. Catal. 125 (1990) 445–455.